First Quarterly Progress Report
NO1-DC-6-2111

The Neurophysiological Effects of Simulated Auditory Prosthesis Stimulation

P.J. Abbas, J.T. Rubinstein, C.A. Miller and A.J. Matsuoka

Department of Otolaryngology - Head and Neck Surgery
The University of Iowa College of Medicine
Iowa City, IA 52242

January 29, 1997

Contents

List of Figures

1 Introduction

Despite the substantial successes that have been demonstrated with cochlear implants, there clearly are limitations in the transfer of information to the central nervous system in individuals using these devices. We suggest that at least some of these limitations are related to spatial and temporal interactions occurring at the auditory nerve with all current designs of implanted prostheses. The project's research program is aimed toward the eventual development of alternative means of stimulating the auditory nerve. Our approach is to use computer simulations and experimental data to:

1. Characterize the fundamental spatial and temporal properties of intracochlear stimulation of the auditory nerve.
2. Evaluate the use of novel stimuli and electrode arrays.
3. Evaluate proposed enhancements in animals with a partially degenerated auditory nerve.

2 Goals accomplished in the first quarter

Personnel for the project have been assembled. We have hired Barbara Robinson to fill the research assistant position at 0.8 time. It was originally proposed that she be hired on the contract only in the third year to prepare histological material. However, we decided that, given her prior experience with our research, her presence now would allow us to be more productive than with a less-experienced person at full time. She began work this quarter.

All equipment requested on the proposal budget has been purchased and is now in place. The Vitalmax 4000-B vital signs monitor has now been used in several experiments, providing status on the animal's core temperature, pulse rate, and pulse oximetry. Together with our CO_2 monitor, it has proven useful in maintaining animals in good physiological condition for extended periods of time. The computer monitor and Pinnacle removable cartridge optical disk have been installed on a Pentium 90 computer to be used with new data collection software that is presently being written by John Todtz. When the initial version of that software is complete, that system will become the primary data collection system in the laboratory. All computers in both the Electrophysiology Laboratory and the Computational

Neurotology Laboratory are now networked so that communication and file access is easily available from all systems.

Preliminary experiments with single nerve fibers are continuing. A new animal headholder was built in-house and vibration isolation added to the sound booth. Both improvements have increased mechanical stability of the preparation, which will extend the "hold" time for collecting single-fiber data. Software has been written for off-line analysis of fiber data which will subsequently be incorporated into the new program for data collection. This software provides stimulus artifact reduction and filtering so that the action potentials can be visualized (see Figure 9) as well as detected. In addition to providing the usual post-stimulus time (PST) histogram data, it performs statistical analyses for the computation of mean latency and temporal jitter. In this reporting period, primary emphasis was placed on acquiring the basic response properties of the electrically evoked compound action potential (EAP). Collection of that data would usually require most of the 24 - 36 hour experimental session. Prior to collecting that data, most cat preparations were also used to acquire single-unit data. Greater emphasis on single-unit data collection will occur with the completion of the data collection software currently under development.

Progress in applying our computational model of the spiral ganglion has been made on a number of fronts. The code implementing the exact solution for a distributed axon with 4000 Na channels per node of Ranvier has been optimized for the architecture of our Silicon Graphics Power Indigo 2 workstation. Thus, small, short simulations may now be run locally, while larger ones are executed on the Cray C90 at the San Diego Supercomputer Center. We have also successfully coded the approximation algorithm of Fox and Lu (1994) for a distributed axon which provides at least a two order of magnitude decrease in calculation time. Because no formal proof exists for determining when the Fox-Lu approximation is valid, the exact solution must still be used regularly to test the accuracy of the approximation.

After the proposal for the contract was submitted, we continued to collect pilot data on both the EAP and single-unit responses. Since the beginning of the contract period, we have run experiments on 3 cats and 5 guinea pigs. This progress report includes data collected before initiation of the contract combined with those experiments done during the first quarter. EAP data

from a total of 10 cats and 14 guinea pigs are included below. Significant single-unit data were collected from a total of 17 fibers in 4 animals.

3 Basic Properties of the EAP

The completed experimental measures of the EAP have focussed on fundamental response properties of the auditory nerve. We have used a basic stimulus – monophasic current pulses delivered by a monopolar intracochlear electrode – to obtain a better and fundamental understanding of the process of electrical stimulation, site(s) of neural activation, and properties of spike initiation and propagation. Animals are deafened using neomycin sulfate infused through the round window. A single stimulation electrode is placed into the basal turn of the scala tympani through the round window. The auditory nerve is exposed through a defect made in the occipital bone. Recordings of the EAP are made from a ball electrode or using an electrolyte-filled glass pipette. Details of the experimental preparation are provided in the Appendix. EAP measures include:

1. EAP growth characteristics: threshold, slope, and dynamic range. The amplitude of response to a single pulse is measured as a function of current level. Threshold, defined by the stimulus level evoking a criterion response amplitude, provides a measure of stimulus efficiency. Input/output amplitude and slope, which likely correspond to the extent of neural recruitment, provide a measure of the spread of excitation across the nerve fiber population. Dynamic range, defined as the range of stimulus levels between threshold and asymptotic (maximum) response amplitude, relates to the usable range of stimulus levels available to recruit the nerve fiber population. Finally, information relevant to the sites and mechanisms of excitation may be gained from both the latency and morphology of the EAP waveform.

2. Strength-duration characteristics: EAP threshold is expressed as a function of stimulus pulse duration in order to obtain strength-duration functions for each of the proposed stimulus waveforms. These functions characterize the integrative properties of the excited fibers (Hill, 1936; Bostock, 1983) and allow us to more fully examine the efficiency of each stimulus over a range of pulse widths consistent with those used in current prosthetic designs.

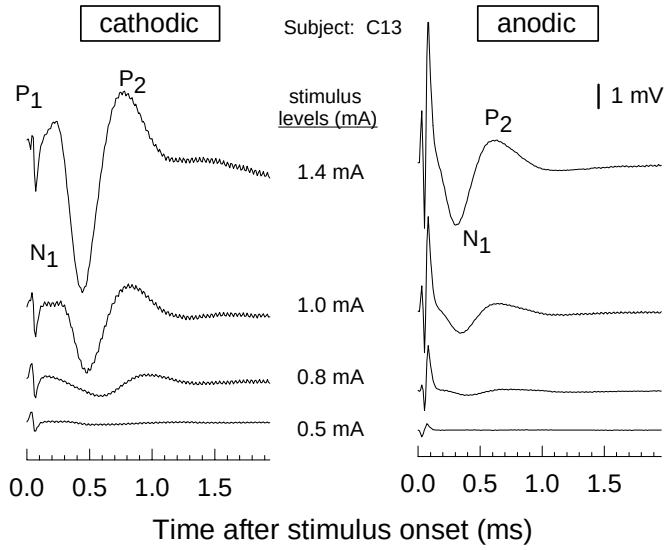

Figure 1: Examples of EAP response waveforms

3.1 EAP waveforms

EAP responses measured from the auditory nerve of a cat are illustrated in Figure 1. Responses to cathodic stimulus pulses are typically triphasic waveforms (peaks P_1, N_1, and P_2) while responses to anodic pulses are typically biphasic (peaks N_1 and P_2). The amplitude of response, measured from the minimum at N_1 to the maximum at P_2, increases with stimulus current level, while the latency of each peak decreases with current level. For equivalent response amplitudes, the latencies of the N_1 and P_2 peaks in response to cathodic stimulation are greater than that for anodic stimulation.

3.2 Growth functions

The trends seen in Figure 1 are explicitly seen in the EAP growth and latency functions of Figure 2. The lower graph plots amplitude of response as a function of stimulus level. The upper graph plots the latency of N_1 and P_2 across the same range of levels. The increase in amplitude and decrease in latency are typical of our data. The differences in both latency and amplitude of the response to the two stimulus polarities are also typical.

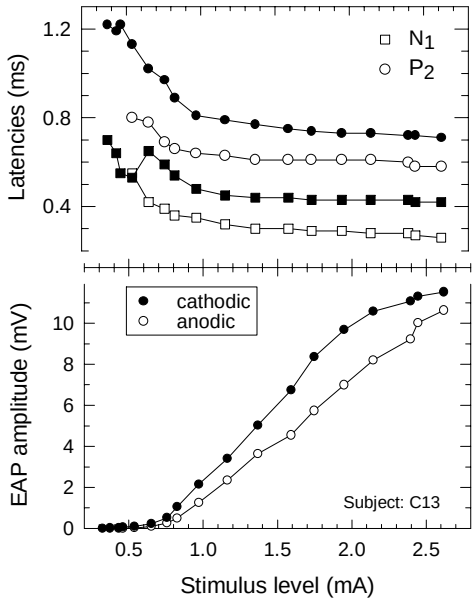

Figure 2: EAP growth and latency functions from a cat

Examples from two guinea pigs, shown in Figure 3, demonstrate variations in the form of the growth functions that we have encountered. Most growth functions show a saturation at high stimulus levels (G45, anodic; G52, cathodic). In a few cases, functions continue to increase at high stimulus levels where the response to the opposite polarity has clearly saturated (G45). In some cases, we have observed a nonmonotonic growth function where, after reaching an apparent saturation, the response decreases with further increases in stimulus level (G52, anodic).

These complexities in the shape of EAP growth functions makes it difficult to characterize each curve by a single value. However, as a first attempt to do so, we have measured a "maximum slope" for each growth function. A piecewise linear approximation results in a measure of slope that varies across stimulus level. The peak in that function is indicative of the highest slope reached for each function. Maximum slope data for the groups of

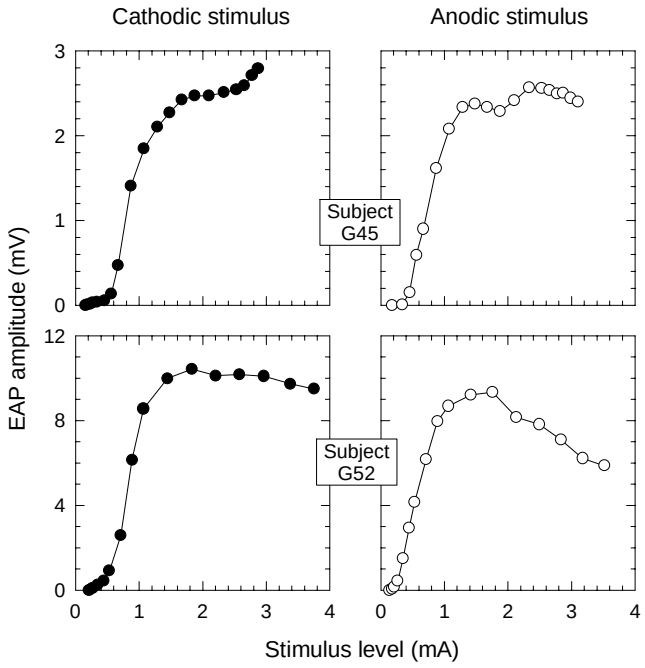

Figure 3: EAP growth functions from two guinea pigs

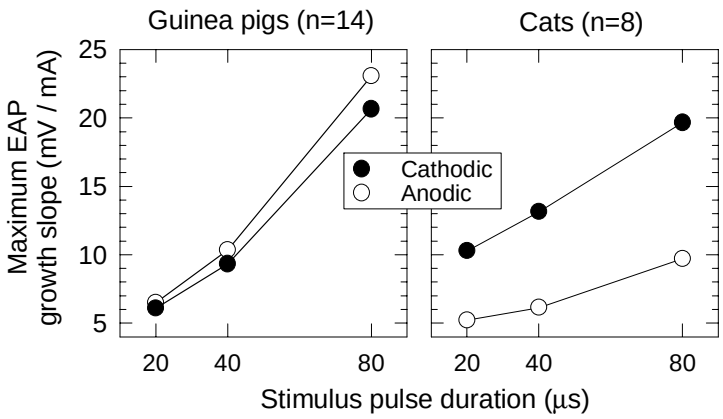

Figure 4: Group data for maximum slope of the EAP

guinea pigs and cats are summarized in Figure 4. Plots of maximum slope versus pulse duration show that the slope of the growth function consistently increases with pulse duration. While the guinea pig data indicates no significant differences in the slopes as a function of stimulus polarity, a relatively large polarity difference is observed in the cat data. At this point, with data from a small number of cats, a t-test of these differences indicates an appreciable chance ($p = 0.10$) that there is no significant difference with polarity. Additional data from future cat experiments will increase the statistical power for better resolution of this question.

3.3 Threshold data

The point on the growth function at which a criterion response is reached is defined as threshold level. Summary data on threshold values for both cats and guinea pigs are illustrated in Figure 5. These data were obtained using monophasic pulses 20 μs in duration; a criterion response amplitude of 100 μV was used to define threshold. The grouped guinea pig data indicates that cathodic stimuli requires a higher level to achieve threshold than does anodic stimuli. A paired-comparison t-test of the guinea pig data indicates this is a significant trend ($p = 0.009$). In the cats, there appears to be a trend in the opposite direction (i.e., cathodic thresholds lower than anodic thresholds). In this data set, however, the difference is not statistically

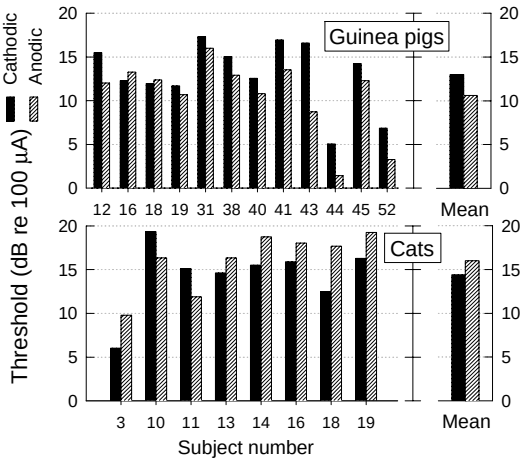

Figure 5: Group data for EAP threshold

significant. We should note that threshold data obtained from the unit responses of 14 single fibers does indicate a statistically significant difference in polarity in the same direction as the cat EAP data (see discussion in Section 4: Single fiber and model results).

3.4 EAP latency

The trends in EAP latency noted above are summarized in the group data in Figure 6. The data of this figure are plotted as a function of EAP response amplitude so as to afford comparison across animals with differing sensitivities and characterize latency at uniform response amplitudes across subjects. The upper graphs plot the latency of N_1 and P_2 peaks versus response amplitude. Latency tends to decrease slightly as EAP amplitude is increased. For both guinea pigs and cats, latencies obtained for cathodic stimulation is consistently greater than that for anodic stimulation. The shape of the EAP wave also shows some variation as a function of stimulus level and polarity. Those trends are summarized in the lower two graphs which plot the EAP width (N_1 - P_2 interpeak latency difference) as a function of response amplitude. In most cases, the EAP width decreases with increasing response level. Across polarities, there is a trend in the cat data for larger EAP widths for cathodic stimulation, although it is not statistically significant ($p = 0.13$) in this set of cat data.

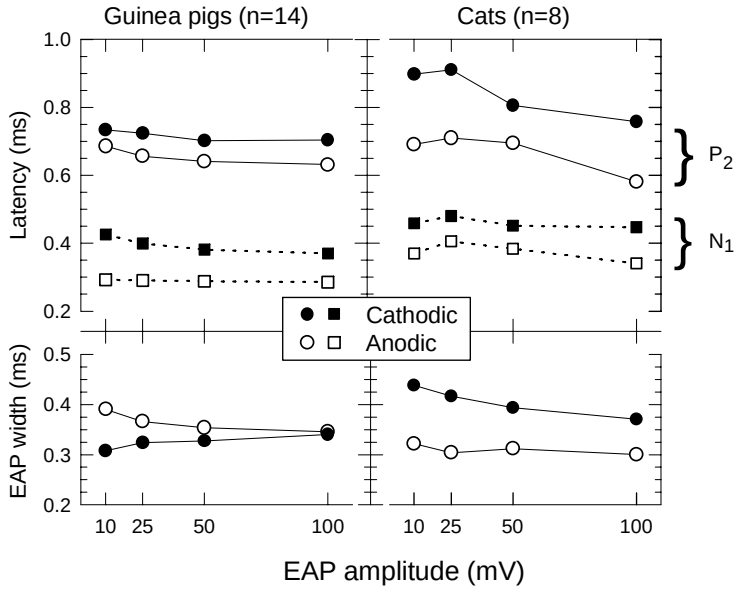

Figure 6: Group data for EAP latency and width

3.5 Strength-duration functions

Examples of EAP strength duration functions from a guinea pig are shown in Figure 7. Threshold of response is plotted as a function of pulse duration for both cathodic and anodic stimulation. Note that the data are plotted on logarithmic axes. At these short pulse durations, this transformation enables us to characterize the slope by linear regression with good accuracy (c.f. Miller et al., 1995). The polarity-dependent trend in guinea pig thresholds, noted above, is seen here at all three stimulus levels. The line segments of Figure 7 indicate the linear regressions to the data. The slope of these lines are different for the two polarities; cathodic shows a smaller change in threshold as pulse duration is changed. The same polarity dependence is suggested in the group data of both cats and guinea pigs (Figure 8), where the slopes of the strength-duration functions are shown for both cathodic and anodic stimuli for each animal. There is appreciable variability in the data however, and the mean differences in the two groups are not statistically significant (guinea pigs: $p = 0.09$; cats: $p = 0.17$). The slope of the strength-duration function, is likely related to the membrane time constants

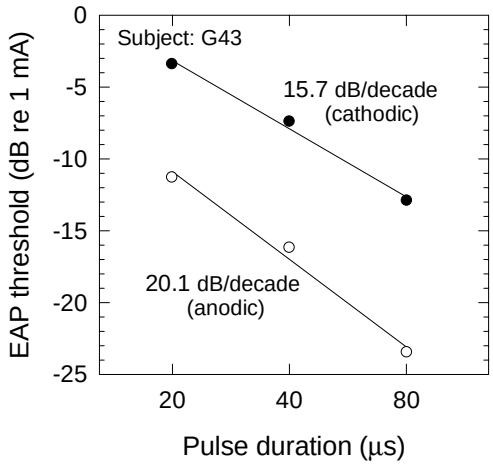

Figure 7: Examples of EAP strength-duration functions

of the responding nerve fibers. The dependency of this measure on polarity is consistent with the notions that different stimulus polarities excite different longitudinal regions of auditory nerve fibers and that the electrical characteristics of those fibers vary longitudinally.

3.6 Summary of EAP data

The data collected thus far characterizes the EAP threshold, growth, and strength-duration characteristics in response to monophasic stimuli delivered by a monopolar electrode. A number of differences have been noted in the responses to anodic and cathodic stimuli and are listed here along with corroborating figures:

- waveshape (Figure 1)
- latency of response (Figures 2 and 6)
- slope of growth function (Figure 3)
- threshold of response (Figure 5)
- EAP width (Figure 6)
- slope of the strength-duration function (Figure 8)

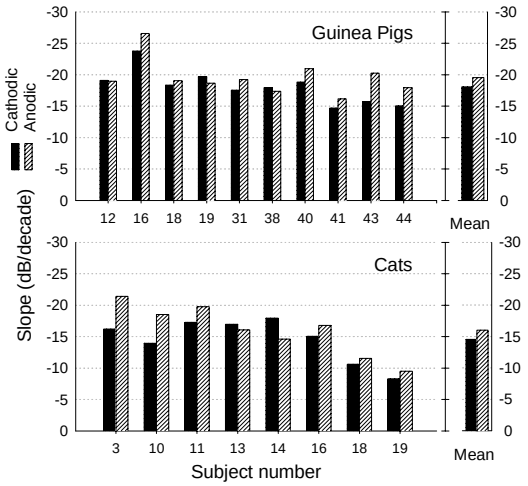

Figure 8: Group data for slopes of strength-duration functions

In addition, we noted variations in the shape of growth functions across subjects – in particular, the occurrence of nonmonotonic growth functions in some subjects.

4 Single fiber and model results

One goal of our initial work on this contract is to provide a better understanding of the characteristics of EAP response in terms of the underlying single fiber response properties. We will pursue this in two ways: first, through direct recordings of single fibers in the same animals EAP data is collected, and second, through the use of the anatomically based, stochastic model of the nerve response. In this section, we address each of the observations of EAP response made above in terms of the underlying single fiber response properties and model characteristics. At this time, the single fiber data is sparse; nevertheless, the data does illustrate how single-unit responses may enhance our understanding of EAP response characteristics. In the data discussed below, the stimulus used was a 20 μs, monophasic pulse delivered by a monopolar intracochlear electrode.

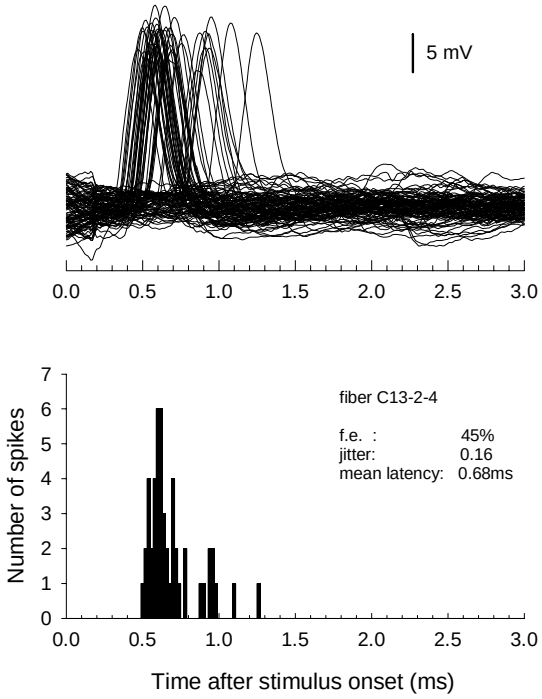

Figure 9: Example of single fiber responses (top) and corresponding PST histogram

4.1 Examples of single fiber responses

Figure 9 shows examples of recorded responses to 100 single-pulse stimuli superimposed on one another. The stimulus artifact has been blanked out of each trace. The calculated PST histogram based on these traces is plotted below the responses. Three variables that are typically used to quantify these responses are indicated on the histogram. The firing efficiency (f.e.) indicates the percentage of presentations for which an action potential occurs. Unit threshold is defined as the level at which f.e. is 50%. We measure latency by the time difference between the onset of the stimulus and the peak of the action potential. The mean latency is the average latency value of those traces in which an action potential occurs. Jitter, the standard deviation of the distribution of spike latencies, is a measure of the temporal dispersion of the fiber's response.

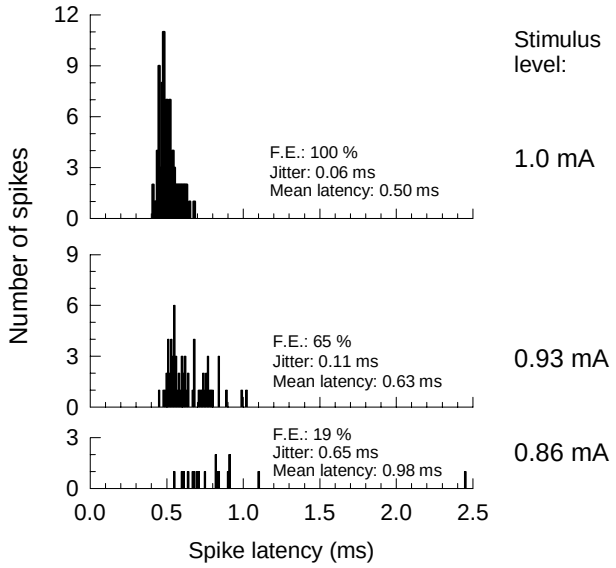

Figure 10: Single-fiber histograms at three stimulus levels

Figure 10 shows histograms from a single fiber for three levels of stimulation. The plots indicate trends that we have observed in that both latency and jitter decrease with increasing stimulus level. These trends are at least qualitatively consistent with EAP data shown in Figures 1 and 2.

4.2 Effects of stimulus polarity on response latency

Like the EAP, the response of single neurons is dependent on the polarity of pulsatile stimulation. The left panels of Figure 11 show PST histograms in response to cathodic and anodic stimulus pulses; the right panels depict EAP waveforms obtained from the same cat. All data of this figure were collected using 1.0 mA, 20 μs pulses. The anodic stimulus, as is typical, results in a shorter mean single-fiber latencies. The EAP waveforms reveal a similar effect in N_1 and P_2 latencies. The N_1 latency difference between cathodic and anodic stimulation is 0.14 ms; the P_2 latency difference is 0.19 ms. These values are comparable to the single-fiber latency difference, which is 0.24 ms. Such polarity-dependent single fiber data are also consistent with the EAP responses discussed above (Figures 2 and 6).

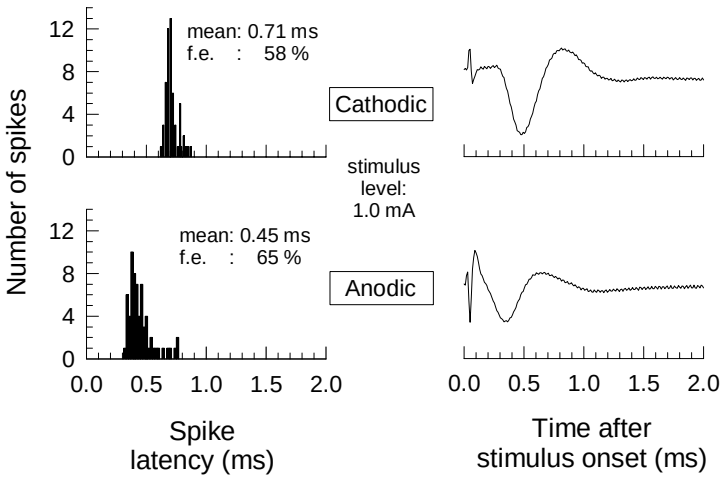

Figure 11: Comparison of single fiber histograms with EAP responses in the same subject

4.3 Growth of response with stimulus level

Figure 12 illustrates three examples of single fiber input-output functions from a cat, along with its corresponding EAP growth function. In each case, firing efficiency is plotted as a function of stimulus level. Each fiber has a limited dynamic range, but there is considerable difference in the sensitivity across fibers within the subject. The EAP growth function has a relatively wide range, suggesting that the EAP growth function encompasses the dynamic range of many individual neurons. This process is demonstrated in Figure 13 where a series of simulated Gaussian input/output functions with narrow dynamic range ($RS = .04$) but thresholds varying by a factor of two, sum to produce a normalized growth function with much wider dynamic range (Compound $RS = .29$).

Figure 14 illustrates another property of single neuron responses which may affect EAP growth. Firing efficiency, jitter, and mean latency of a cat fiber are all plotted as functions of stimulus level. The growth of firing efficiency with level is accompanied by a decrease in the other two variables. We observe, however, that at levels where firing efficiency has saturated at 100%, jitter continues to decrease. If one considers that the EAP is related to

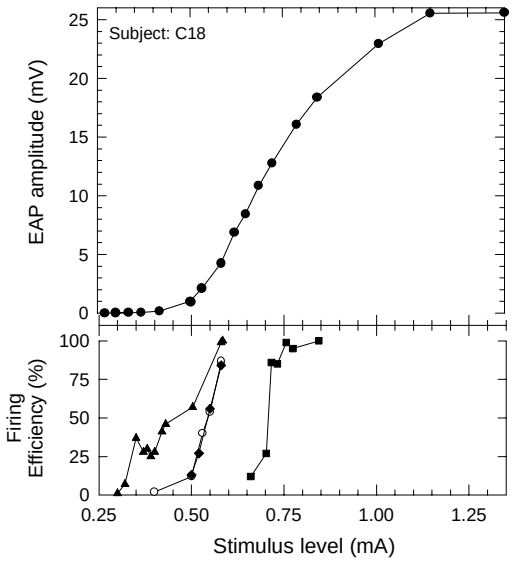

Figure 12: Comparison of EAP and single fiber growth functions

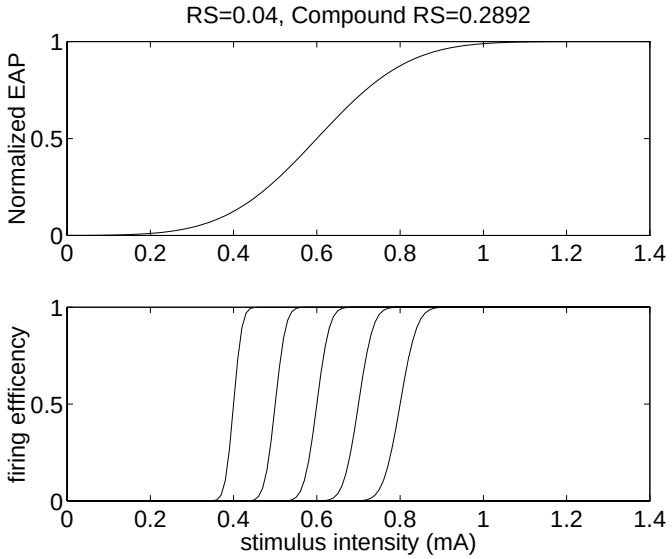

Figure 13: Simulated Gaussian input-output functions and calculated EAP growth functions

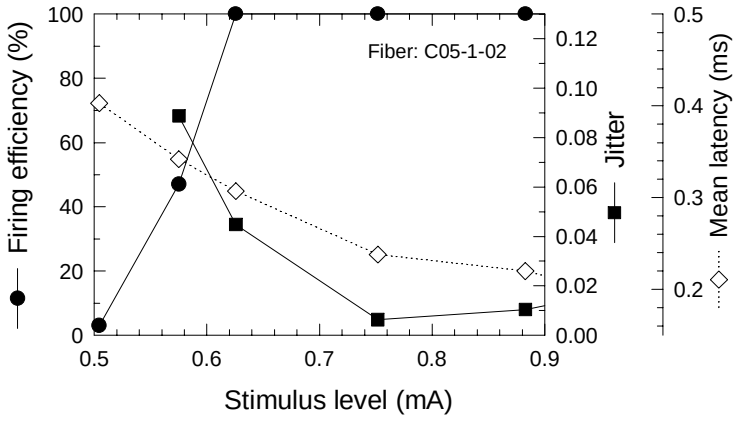

Figure 14: Firing efficiency, mean latency and jitter plotted versus stimulus level for a single fiber

both the number (firing efficiency) of active neurons and also the synchrony (jitter) of those responses, then these data suggest that individual fibers may contribute to continued growth of the EAP beyond levels at which firing efficiency saturates. Simulations using a multiple-neuron model to calculate EAP responses are illustrated in Figure 15. These data show firing efficiency and jitter for the underlying neuron responses as a function of stimulus level in addition to the calculated EAP amplitude. Like the animal data of Figure 13, the model also shows a significant decrease in jitter at firing efficiencies very near 100%. At these higher stimulus levels, increases in EAP amplitude results from increased synchrony (i.e., decreased jitter) rather than increased neural recruitment.

4.4 Location of spike initiation can affect EAP waveshape and integrative properties

Results from the single fiber model which includes a cell soma that were reported in Rubinstein and Dynes, 1993, and in the contract proposal demonstrate that the initiation of the action potential occurs at a peripheral site for cathodic stimulation and at a site central to the cell soma for anodic stimulation. This observation is consistent with single fiber and EAP latency data reported here (Figures 1, 2, 6, and 11).

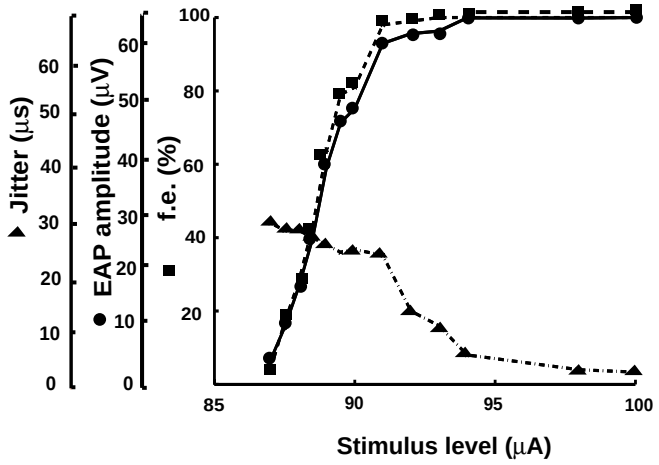

Figure 15: Model calculations of EAP amplitude, single fiber f.e., and jitter

Furthermore, a different site of stimulation would be consistent with other observations listed above. For instance, the conduction of action potentials through the cell soma results in greater jitter (demonstrated by the model) consistent with a greater EAP width for cathodic stimuli in the cat (Figure 6).

Threshold data from single fibers collected thus far in cats is consistent with the trends observed for the EAP. Figure 16 plots the cathodic and anodic thresholds for 14 fibers, revealing a strong trend for lower cathodic thresholds. Note that in cases marked with an asterisk, threshold was not achieved at the level indicated. The level shown is the highest tested, indicating that the threshold level is at least that high. A paired-comparison t-test of the cathodic and anodic latencies of these 14 fibers indicates it is highly significant ($p = 0.0007$) trend. This finding is in accord with the EAP findings discussed above. Model calculations demonstrate that cathodal threshold is lower, latency is longer, and time constant is greater than corresponding values attained with anodal stimulation. These results are all consistent with both single fiber and EAP recordings. Nevertheless, single-fiber thresholds are likely dependent on the location of the stimulating electrode relative to the neuron, in addition to specific membrane characteristics of the peripheral and proximal axonal processes. The opposing polarity effects seen in the group EAP thresholds for guinea pig and cat (Figure 5),

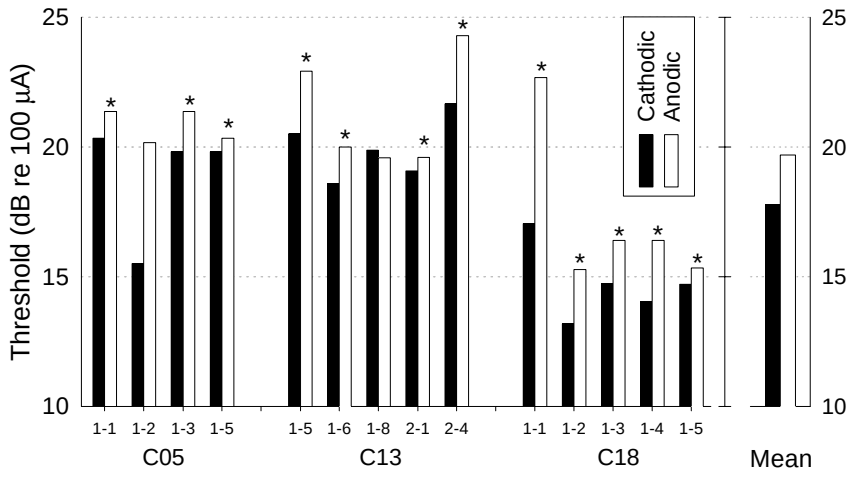

Figure 16: Summary data for single-fiber threshold levels

for example, may be the result of such interspecies differences.

Membrane properties at the peripheral dendrite are likely different than those at the nodes on the central axon. The strength-duration slope data imply that different membrane time constants are effective for anodic and cathodic stimulation. This observation is not only consistent with the model, but also with the single-fiber recordings of van den Honert and Stypulkowski (1984) obtained with cathodic stimuli before and after laminectomy. Their observations of reduced latencies and membrane time constants after laminectomy are consistent with a shift in place of spike initiation. Anodic stimulation of an intact spiral ganglion cell likely excites the neuron somewhere near the laminectomy site.

5 Plans for the next quarter

In the next quarter, we plan to continue to refine our single-fiber recording techniques to improve mean times for maintaining unit potentials. For each cat experiment, we will continue our protocol of devoting the first 6-8 hours of experiment time to single-fiber data collection, after which the remaining time will be devoted to EAP recordings.

Data on threshold, growth, and strength-duration will be collected on several more subjects in order to complete the data set that was, in large measure, discussed here. Data have been collected on temporal response properties, including conditioning and refractory properties and responses to pulse trains. Those data will be analyzed and additional data collected during the next quarter. In addition, initial data on spatial interactions using multi-electrode arrays will be collected.

Upcoming computational efforts will focus on simulations of large populations of fibers as well as demonstrating the effects of refractoriness on membrane noise. The very large scale simulations use the Fox-Lu approximation on the parallel IBM SP-2, while smaller studies of refractoriness (100 or so fibers) will use the Fox-Lu algorithm on our local workstation. The exact solution for 100 fibers on the vector Cray C90 will remain the benchmark to ensure accuracy of the approximation.

The Fox-Lu approximation appears to give statistically identical results to the exact solution for PST histograms and EAP growth functions as long as there are more than 800 Na channels per node of Ranvier. The dramatic increase in computational speed provided by the approximation allows the simulation of large numbers of fibers for longer periods of time. It holds promise of simulating an entire auditory nerve (30,000 fibers in the human) for periods of time of interest in speech processing (tens of milliseconds). In pursuit of this goal, we have successfully ported the approximate solution to both our SGI workstation and the 100 GFlop IBM SP-2 at the Maui High Performance Computing Center. Our workstation allows modeling 100 fibers over 2 milliseconds in about 4 minutes. The SP-2 has simulated 30,000 fibers over 1 millisecond in about twelve minutes. We currently have no good way to manipulate this massive solution as it is over 1 gigabyte in size, but expect to have the appropriate software tools in place during the next quarter. A 26800 fiber PST histogram calculated by the SP-2 is shown in Figure 17.

Finally, we will present results of this work at the Midwinter Meeting of the Association for Research in Otolaryngology (February 1-6, 1997) in three podium presentations.

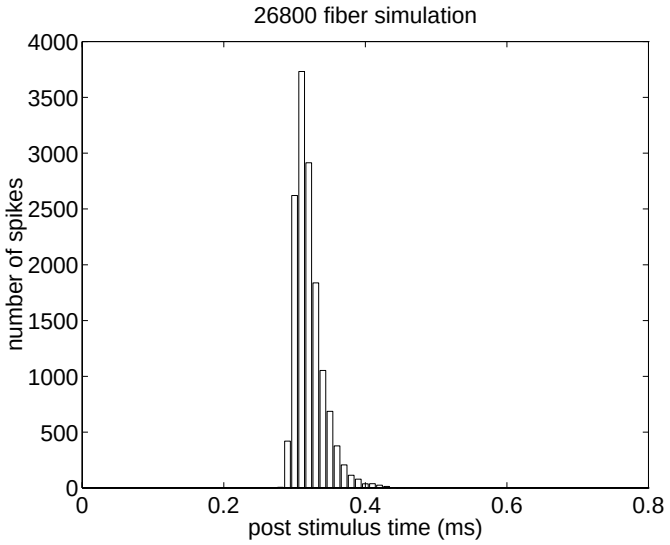

Figure 17: A 26800 fiber PST histogram calculated by the SP-2

A Methods used in the acute animal experiments

A.1 Anesthesia and monitoring

For the cat experimental sessions, animals are first sedated with a combination of ketamine (20 mg/kg) and acepromazine (0.2 mg/kg). After shaving areas of skin for surgical access, the femoral vein is catheterized and a saline drip (2 ml/kg/hr) established for hydration. Pentobarbital anesthesia is also administered through this route, with an initial dose given to effect (approximately 8 mg/kg). For the guinea pig, we use a three-way combination of ketamine (40 mg/kg), xylazine, (7.5 mg/kg), and acepromazine (0.5 mg/kg). Maintenance doses of approximately one-third to one-half this initial dose will be given as needed, at approximately 45 to 90 minute intervals. For guinea pigs, hydration is provided by subcutaneous injections of saline (15 ml/kg/4hr). After anesthesia is induced, areas around the trachea and head are locally anesthetized with subcutaneous injections of lidocaine with epinephrine. The animal is tracheotomized and connected to a Harvard Apparatus animal ventilator connected to an oxygen supply. The animal is kept warm with a circulating water heating pad and drapes. For cat preparations, the head is then secured to the experimental table by a custom-built head-holder.

Vital signs are monitored and recorded throughout the experiment to ensure stability of the preparation. Core temperature, heart rate, and blood oxygen saturation are monitored by a vital signs monitor (Pace Technologies) as is expired partial pressure of CO_2 using a capnometer (Traverse Medical Monitor). For both species, subsequent anesthetic doses are administered in response to several indicators, including pedal reflex, respiration pattern, and core temperature elevation. All surgical and experimental procedures have been approved by the University of Iowa Animal Care and Use Committee.

A.2 Surgery

To access the middle ear and auditory nerve, an incision is made to expose the posterior aspect of the left side of the skull. In the cat, this incision forms a crescent from the medial insertion of the pinna posteriorly to midline and then laterally toward the jugular process. In the guinea pig, an incision is made from the midline near the orbits, through bregma, and laterally to the mastoid region. For both preparations, skin flaps are retracted to

expose the auditory bulla and lateral region of the occipital bone. For guinea pigs, the skull around bregma is exposed and the periosteum removed to facilitate mounting a head-holding screw. Three small (#6-32) screws are first threaded into the skull such that they surround the head of a larger (#2-56) screw, which is cemented to the three screws with methyl methacrylate. The large screw is then bolted to a fixture which immobilizes the guinea pig's head. For both species, muscle overlying the bulla is removed and a small defect is made in the bulla with a cutting burr to expose the middle ear and round window. The membrane of the round window is removed and perilymph is carefully aspirated from the cochlea. Perilymph is replaced with 50 ml of 10% (weight/volume) Neomycin sulfate solution infused slowly into the cochlea. This is done in stages with a microsyringe, with repeated aspiration between infusions. This infusion of antibiotic serves to kill hair cells to abolish electrophonic responses.

After deafening, a defect is made in the skull to expose the auditory nerve. This exposure is somewhat different in each species. In the cat preparation, muscle attachments to the occipital ridge are cauterized and the bony ridge is opened with a rongeurs. The defect is enlarged to expose the left, lateral aspect of the cerebellum. The dura is carefully cut and retracted, taking care to avoid bleeding. Small cotton balls are used to retract the cerebellum medially to expose the auditory nerve near the porus acousticus. In the guinea pig, the temporal bone is thinned medial to the acoustic meatus around the temporal line. Bone is removed using fine rongeurs to expose the flocculus, which is then cauterized or retracted. Care is taken to avoid bleeding or tearing the dura. The brain is retracted with cotton balls to expose the auditory nerve, which lies posterior and ventral to the vestibular nerve.

After surgical exposure, the head is locked into position and stimulus and recording electrodes are placed. The stimulating electrode (or array) is positioned into the basal turn of the cochlea via the round window. The return electrode is positioned on bone within the middle ear cavity, on the ventral aspect of the bulla. For EAP recordings, a Pt/Ir ball electrode (diameter: 0.25 mm) is placed in contact with the auditory nerve and connected to the positive input of a differential amplifier. A return electrode (negative input) is positioned between cranial bone and brain several (i.e., at least 5) millimeters from the nerve trunk. A needle electrode is inserted into neck muscle

to establish the amplifier ground path. For single-fiber recordings, 1 mm micropipettes are pulled and filled with 3M KCl solution. Only pipettes with impedances (measured using a 22 Hz square wave) greater than 15 MΩ are used. The pipette is connected to an Axon Instruments unity-gain headstage using a return electrode similar to that described above. Amplification, capacitive compensation, and 10 kHz low-pass filtering are provided by an Axon Instruments Axoprobe amplifier.

A.3 Stimulus generation

Stimuli are generated by a 12-bit digital-to-analog converter operating at a rate of 100 000 samples/s and controlled by in-house software. A custom-made, battery-powered, optically isolated current source is used for stimulation. Throughout the experiment, stimulation current is monitored on an oscilloscope for calibration purposes. The rise-fall time of the current source is approximately 10 μs. This results in some distortion of the desired rectangular wave shape. To account for this when stating the pulse amplitude, the actual current delivered by each stimulus is computed using a correction factor based on the area of the waveform. All stimulus levels are expressed as a equivalent baseline-to-peak amplitude of the rectangular pulse. Two measures are used to prevent passage of direct current to the tissue. The stimulating electrode is capacitively coupled to the current source. Also, all monophasic stimuli are presented in a sequence in which cathodic (negative) and anodic (positive) pulses are interleaved. Throughout this study, the stimulation rate is expressed by the interstimulus interval (ISI), which is the time between onsets of sequential cathodic and anodic pulses. Thus, the time between successive pulses of the same polarity is twice that of the ISI. Unless otherwise noted, an ISI of 18 ms was used in the collection of the data described in this report.

Stimuli are presented either through an intracochlear electrode built in-house or (in later reporting periods) experimental multiple-contact arrays provided by Dr. Loeb. In the case of the former, the electrode is formed by flame-balling a 0.005" diameter Pt/Ir wire to a diameter of 0.35 - 0.45 mm and then insulating the shank. The wire is then threaded through catheter tubing for greater rigidity. Prior to use in an experiment, the surface area of the ball is enhanced by inducing the formation of a surface hydride layer using a technique suggested by the work of Brummer and Turner (1977). This procedure reduces the measured impedance of the Pt/Ir

electrode typically by at least 50% and increases the level of current that can be delivered without the risk of in vivo electrolytic reactions.

A.4 Response recording

EAP potentials are first amplified by a custom-built differential amplifier (20 dB gain). The signal is then passed first through a 6-pole Butterworth low-pass filter (3 dB frequency = 30 kHz) and then to a 16-bit analog-to-digital converter sampling at a rate of 100,000 samples/s. The responses are then recorded using standard signal-averaging techniques using custom software. Typically, 4000 to 100 sweeps are used in each averaged response, depending upon signal-to-noise conditions as determined by the experimenter.

Single-fiber potentials are first sent to a unity-gain headstage and then amplified (40 dB) and low-pass filtered (2-pole, 3 dB frequency = 10 kHz) by stages within the Axon Instruments Axoprobe amplifier. The signal is then sampled by the same equipment used in the EAP recordings. Currently, we record each post-stimulus record of each stimulus presentation and store the waveforms to disk. The waveforms are analyzed off-line using a custom-written Matlab routines. These routines eliminate stimulus artifact by the use of a template subtraction procedure (i.e., using a trace in which no action potential occurs as a template that is subtracted from all traces) and simple blanking of each trace. Spike detection is then performed by classic window discrimination; the peak of each action potential is used to define its latency. The program also computes statistics such as firing efficiency, mean latency, and jitter.

References

[1] Bostock H. (1983). The strength-duration relationship for excitation of myelinated nerve: Computed dependency on membrane parameters. J. Physiol., 341, 59-74.

[2] Brummer, S.B. and Turner, M.J. (1977) Electrical stimulation with Pt Electrodes: I - A method for determination of "real" electrode areas, IEEE Trans. Biomed. Eng. 24, 436-439.

[3] Fox, R.F. and Lu, Y-n. (1994) Emergent collective behavior in large numbers of globally coupled independently stochastic ion channels. Phys. Rev. E, 49(4), 3421-3431.

[4] Hill A.V. (1936). Excitation and accommodation in nerve. Proceed. Royal Society of London. Series B: Biological Sciences., 119, 305-355.

[5] Miller, C.A., Woodruff, K.E., and Pfingst, B.E. (1995) Functional responses from guinea pigs with cochlear implants. I. Electrophysiological and psychophysical measures. Hear. Res. 92, 85-99.

[6] Rubinstein J.T., & Dynes S.B.C. (1993). Latency, polarity and refractory characteristics of electrical stimulation: Models and single-unit data. Abstracts of Assoc. Res. Otolaryngol.

[7] van den Honert C., & Stypulkowski P.H. (1984). Physiological properties of the electrically stimulated auditory nerve. II. Single fiber recordings. Hearing Res., 14, 225-243.